Engineering Structures 214 (2020) 110681

Contents lists available at ScienceDirect

Engineering Structures

journal homepage: www.elsevier.com/locate/engstruct

Wind-induced response characteristics of a yawed and inclined cable in ABL wind: Experimental- and numerical-model based study

Mohammad Jafari, Partha P. Sarkar*

Aerospace Engineering Department, Iowa State University, Ames, IA 50011, USA

ARTICLE INFO

Keywords:
Aeroelastic cable model
Dry galloping
Wind-induced vibration
Inclined cable
Aerodynamic cable damping
FEA of cable

ABSTRACT

Inclined cables used in bridges or other infrastructures are vulnerable to unsteady wind-induced loads producing moderate- to large-amplitude vibration that may result in damage or failure of the cables, resulting in catastrophic failure of the structure they secure. In the present study, wind-induced response of an inclined smooth cable was studied through wind tunnel measurements using a flexible cable model for a better understanding of the vibration characteristics of structural cables in atmospheric boundary layer wind. For this purpose, in-plane and out-of-plane responses of a sagged and a non-sagged flexible cable were recorded by four accelerometers. Four cases with different yaw and inclination angles of a cable with approximate sag ratios of 1/10 were studied to investigate the wind directionality effect on its excitation mode(s) and response amplitude. Cable tension was also measured during all experiments to assess the correlation of wind speed, excitation vibration mode, and natural frequency of the cable with change in cable tension. Additionally, two inclined cables with no sag were tested to determine the influence of sag of a cable on its vibration characteristics. In the second part of this study, a series of finite element analyses were conducted to predict the wind-induced aerodynamic damping of an inclined bridge cable. Experimental results showed that excitation mode(s) of a cable depend on wind speed, inclination angle, and sag ratio and cable tension. First, second, and third vibration modes were observed at a low wind speed for different test cases, whereas higher vibration modes were observed to contribute to the cable response at high wind speeds. Moreover, it was seen that the cable tension significantly increased with wind speed resulting in increased value of the excited natural frequency. Numerical results obtained through finite element analysis of an inclined full-scale cable showed that the criteria that are based on section models can underestimate the critical reduced velocity for dry cable galloping.

1. Introduction

Wind can induce moderate- to large-amplitude low frequency oscillations in structural cables that are used to support long-span structures such as bridges and roofs. These vibrations can cause failure in cables that could trigger collapse of the structure they support. The aerodynamic instabilities or divergent response of cables are triggered by wind-induced effects that are conventionally classified into vortex-induced vibration (VIV) [1–3], rain-wind induced vibration (RWIV) [4–7], dry, ice and wake galloping [8–11]. These phenomena have been widely investigated through wind tunnel tests and computational fluid dynamics (CFD) to determine the mechanisms and parameters that influence them. Over the past decades, wind-induced vibration of inclined cables has been mostly studied by performing wind tunnel test on section models. These studies often fell short of explaining the observed and measured behavior of a stay-cable in the field. The roles of sag, inclination angle, and tension in the cable and those of the upstream wind such as turbulence and variable mean-wind speed with height in ABL wind have not been fully explored. In this study, the wind-induced response of an inclined aeroelastic-model of a dry cable, with and without sag, was studied in atmospheric boundary layer wind in an open terrain. The effects of different cable parameters such as sag ratio, tension, yaw angle and inclination angle, and their combination on the wind-induced response of a scaled aeroelastic model of the cable were investigated through wind tunnel measurements. In this regard, a new design was used to build the flexible aeroelastic model of the cable in order to better reproduce the response of a full-scale cable.

Over the past decades, dry galloping of smooth cables has been studied either by performing wind tunnel test or numerical simulation to assess the impact of important parameters such as Scruton number (Sc), reduced velocity (RV), and yaw/inclination angles. Matsumoto et al. [12] explained the mechanism of dry galloping in cables through

* Corresponding author.
E-mail address: ppsarkar@iastate.edu (P.P. Sarkar).

https://doi.org/10.1016/j.engstruct.2020.110681
Received 12 November 2019; Received in revised form 12 March 2020; Accepted 16 April 2020

wind tunnel data and using splitter plates with different perforation (or porosity) ratios located behind a yawed cable (non-inclined). Experimental data showed a steady divergent response or divergent galloping for lower perforation or higher-solidity ratios of the splitter plates. Jafari and Sarkar [13] identified the flutter derivatives and buffeting indicial derivative functions of a smooth cable for yaw angles ranging from 0° to 45° using section models subject to free vibration and gust, generated by a gust generator system, in a wind tunnel. They proposed several empirical equations to calculate the wind load parameters of a yawed cable and concluded that an inclined cable with an equivalent yaw angle of 45° is the most critical for onset of dry galloping amongst all yaw angles, where the equivalent yaw of a cable corresponds to the yaw angle of a cable on a horizontal plane equivalent to yaw of an inclined cable on a vertical plane, as defined later. Cheng et al. [14,15] showed the influences of Reynolds number, wind speed, and surface roughness on the response of an inclined cable by measuring the aerodynamic forces in a wind tunnel. The results demonstrated a divergent galloping at a Scruton number of 0.88 and wind speed of 32 m/s. Nikitas and Macdonald [16] measured the wind forces of a cable at different yaw and inclination angles and concluded that inclination angle is a significant parameter. Duy et al. [17] carried out wind tunnel experiment to study the applicability of spiral wires on suppression of dry-cable galloping and observed divergent galloping for yaw angles (β) from 30° to 60°. Yeo and Jones [18] conducted numerical simulation using the detached eddy simulation (DES) turbulence model to explore the effect of yaw angles ranging from 0° to 60°. They found that Karman vortices' strength reduces with increasing yaw angle. Wu et al. [19,20] used a high-fidelity computational fluid dynamics (CFD) technique to capture dry galloping of yawed cable and validated CFD results with experimental data. Raeesi et al. [21] developed a three-dimensional aeroelastic model to calculate the dynamic response of inclined stay-bridge cables subject to unsteady wind loads. They solved the nonlinear equations of motion using finite difference method, and numerical results confirmed the significant effect of critical Reynolds number on dry galloping of yawed/inclined cables.

Wind-induced vibration of flexible cables has been rarely studied in the past due to existing difficulties in building these models to accurately reproduce the response behavior of full-scale cables and also because of limited size of boundary-layer wind tunnel test sections. Literature review shows that only few experimental studies exist on wake-induced, vortex-induced, and rain-wind-induced vibrations of cables using flexible cables. Chen et al. [22] conducted research to investigate the effect of VIV on wind-induced response of a flexible cable with yaw angle of 0° and inclination angle of 25.3° using wind tunnel tests. They measured the cable's acceleration at several locations in cross-flow and in-line directions and observed eight-shape, elliptical, and straight motion trajectories for cable vibration depending on mode shapes. Moreover, they reported the Strouhal number for inclined cable at different heights. Gao et al. [23] captured the multi-modal vortex-induced and rain-wind-induced vibrations of an aeroelastic cable through a series of wind tunnel experiments. Axial force was applied to the cable in order to adjust the natural frequency and minimize the sag ratio. They presented the wind response of an inclined cable by measuring the cable's acceleration in out-of-plane and in-plane directions. First, second, and third vibration modes with dominant peaks were observed at different wind speeds for VIV and RWIV. Additionally, they showed that the motion trajectory of a flexible cable is similar to an ellipse for VIV. Belloli et al. [24] performed wind tunnel tests to measure the vibration of Talavera Bridge in atmospheric boundary layer wind using distributed lumped masses along the original wire to reproduce the flexible cable. They studied the impact of wind direction on aerodynamics of a full bridge and found that the force and moment coefficients on cable's anchorage were maximum when wind perpendicularly approaches the bridge deck. In another study, Khrapunov and Solovev [25] presented wind tunnel results of a full bridge while reproducing the actual cables with steel wire and distributed lumped masses. They proposed a two-step modeling approach to study the aeroelastic instability of full bridges exposed to wind-induced loads. He et al. [8] investigated the effect of elastic cross ties on suppression of wake-induced vibration of staggered cables through wind tunnel experiment on flexible tandem cables. To build the aeroelastic cables, they used steel wires with applied axial force and covered the model by Mass block/Filler and Polyethylene (PE) coating. They measured the acceleration at different locations for a range of reduced velocities and revealed the effectiveness of cross ties on alleviation of wake galloping. While wind-induced fatigue can cause catastrophic damages to the cable-stayed or suspension bridges, Cluni et al. [26] studied the fatigue of suspended cables using wind tunnel tests on a aeroelastic cable with different sag ratios. They also developed a numerical method to use the experimental data and reproduce the cable nonlinearity.

This paper focuses on understanding the wind-induced response of an inclined flexible cable in atmospheric-boundary-layer wind. In this regard, a series of wind tunnel tests were performed to study the effects of different parameters such as sag ratio, wind direction, and wind speed on vibration of a scaled aeroelastic model of a cable. For this purpose, six different cases were tested in a wind tunnel where accelerations of the cable along two directions were measured at two locations along its length. Cable tension was also monitored to study its effect on cable's stiffness or natural frequency as it changed with wind speed. Apart from wind tunnel tests, a finite element analysis was carried out to estimate the aerodynamic damping of an inclined full-scale cable based on parameters derived from two-dimensional section model tests of smooth cylinders. Experiments indicated that excitation mode(s) are dependent on wind speed, inclination angle, and sag ratio. For all cases, first three vibration modes were observed at low wind speeds, while higher vibration modes occurred at high wind speeds. In addition, it was found that the cable tension notably increased with wind speed resulting in increased natural frequency of the cable. By conducting a numerical wind simulation on a finite element model of an inclined full-scale cable in yawed wind, it was shown that the proposed criteria that are based on section models are more conservative in estimating the critical reduced velocity for onset of dry galloping instability.

2. Experimental setup

In this study, wind tunnel experiments were performed in the atmospheric boundary layer (ABL) test section of the AABL Wind and Gust Tunnel (15 m L × 2.44 m W × 1.83 m H) located at Iowa State University. As shown in Fig. 1b, three spires and several wooden blocks with various roughness heights were placed in front of the test section to reproduce the mean wind speed and turbulence intensity profiles of an open terrain. An inclined aeroelastic model of a cable was mounted on an angled ⌊frame with a taut wire running through its center whose tension could be adjusted so as to change the cable's sag and stiffness. Furthermore, the cable's inclination and yaw angles could be adjusted in this test setup by changing the elevation of the upper-end of the cable's connection to the frame and by rotating the turntable on which the frame was fixed. In order to measure the tension in the wire, it was attached to a force balance (JR3®) at its end as shown in Fig. 1b. In all experiments, cable tensile force and cable acceleration data were recorded for 150 s, and their mean or root-mean-square (RMS) values were calculated and presented here.

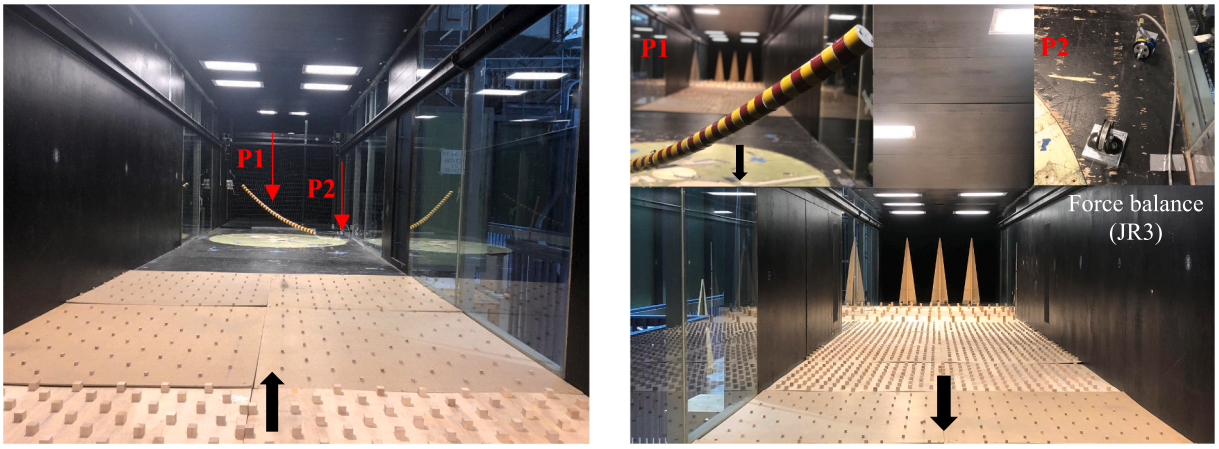

(a) aeroelastic cable model and force balance (b) spires and roughness blocks for terrain

Fig. 1. ABL wind tunnel test setup and aeroelastic cable model.

A novel technique was employed to design and build the aeroelastic cable model in this study in an attempt to capture the realistic behavior of a flexible cable in the field. As shown in Fig. 2, the cable model includes 60 separate segments of solid circular sections made out of blue foam using a CNC or computer numerical control machine. The length and diameter of each segment were 3 cm (1.2 in) and 6.35 cm (2.5 in), respectively, and the total length and mass of the cable model were 2.1 m (6.9 ft) and 0.250 kg (0.55 lb), respectively. A musical wire with a diameter of 0.508 mm was used to assemble all these segments. A metal tube with 5 mm length was used as a spacer to keep enough gap between the segments to allow bending of the cable (see Fig. 2). Although this gap was necessary for cable's flexibility, it was recognized that the incoming flow that would pass through this gap can undesirably distort the aerodynamics of the cable. Therefore, a Monokote sheet that was used to wrap the individual segments to furnish a smooth cable surface was also used to cover the existing gap between the segments by extending it by 4 mm beyond the length of each segment on one side. It should be noted that two additional wires (as shown in Fig. 2) with a minimal amount of tension to keep it taut were placed on opposite sides of the center of the cable segments along the cable length to provide some torsional stiffness to the model in order to avoid cable rotation during the tests.

A schematic view of the inclined aeroelastic or flexible cable model (length scale 1:50 and frequency scale 2), as used in this study, is shown in Fig. 3. Four uniaxial accelerometers were attached to the model in

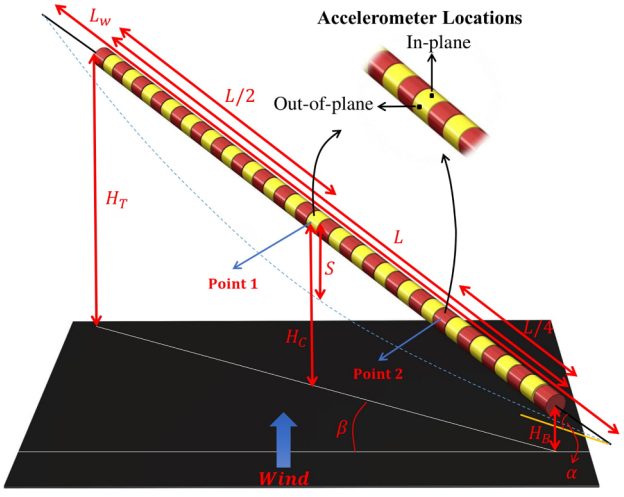

Fig. 3. Schematic view of an inclined model to define the studied parameters.

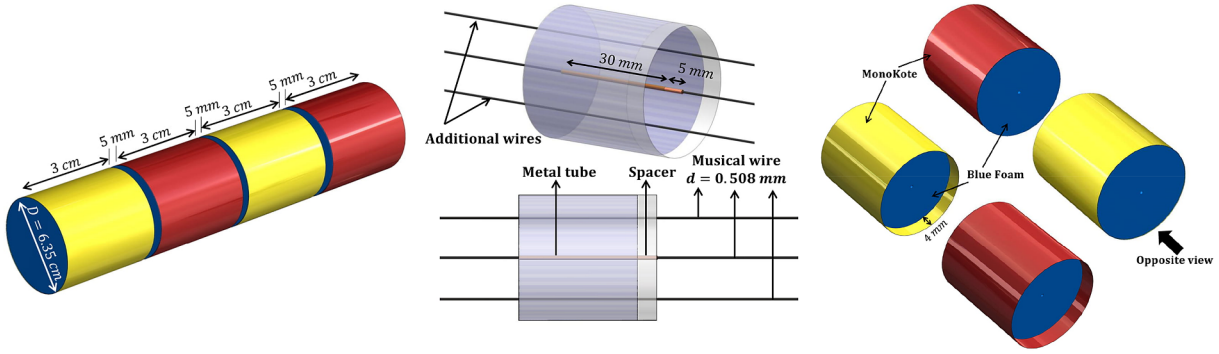

Fig. 2. Dimensions and details of designing aeroelastic model's segments.

order to measure the accelerations at two locations, one pair located at mid-point (Point 1) and another pair at quarter-point (Point 2) along the length of the inclined cable as illustrated in Fig. 3. Two accelerometers at each of the two points were attached, one on the top of cable to measure in-plane accelerations, and the other one on the downwind side of the cable with a 90° orientation compared with the top one. In this study, the normalization of the acccelerations/displacements was done based on measured quantities at Point 1.

For wind tunnel experiments, six different cases were considered to study the effects of yaw (β), inclination (α), equivalent yaw (β^*) angles, and sag ratio (SR) of the cable on wind-induced vibration of an inclined cable for wind speed (U_c) ranging from 0.25 to 10.80 m/s at Point 1.

Table 1
Details of experimental setup and aeroelastic cable tested.

	α°	β°	$\beta^{*\circ}$	SR (%)	H_B(mm)	H_C (mm)	H_T (mm)
Case 1-WithSag	20	38	35	11	102	356	864
Case 2-WithSag	20	49	45	9	76	305	813
Case 3a-WithSag	35	45	35	9.5	127	584	1270
Case 3b-NoSag	35	45	35	0	228	787	1398
Case 4a-WithSag	35	60	45	8.5	152	686	1346
Case 4b-NoSag	35	60	45	0	182	826	1452

Table 2
Measured natural frequencies and measured damping ratio of model.

Case	Direction	First mode (Hz)	Second mode (Hz)	Damp. Ratio ζ
Case 1-WithSag	In-plane	1.16	2.25	0.026
	Out-of-plane	1.12	2.19	0.020
Case 2-WithSag	In-plane	1.12	2.19	0.028
	Out-of-plane	1.10	2.44	0.023
Case 3a-WithSag	In-plane	0.99	1.89	0.025
	Out-of-plane	0.95	1.95	0.019
Case 3b-NoSag	In-plane	3.17	6.22	0.027
	Out-of-plane	3.10	6.06	0.024
Case 4a-WithSag	In-plane	1.42	2.75	0.021
	Out-of-plane	1.35	2.80	0.022
Case 4b-NoSag	In-plane	3.45	6.78	0.025
	Out-of-plane	3.41	6.56	0.023

The in-plane Scruton number (Sc) of the aeroelastic cable is 0.61 based on average mechanical damping of 0.0253 for all cases (see Table 2). The details of these cases are summarized in Table 1, where four test cases are with cable sag and two are without cable sag. The equivalent yaw angle relates yaw and inclination angles of an inclined cable as defined in Eq. (1). Although it was found in past studies [13,27] that equivalent yaw angle of 45° is the most critical yaw angle in the range of 0° to 45° for dry-cable galloping, the influence of another equivalent yaw angle of 35° was also assessed here through Cases 1 and 3a to verify it. Sag ratio($SR = S/L_w$) that is defined as the ratio of maximum cable static-deflection (S) due to cable weight to the total span (L_w) of the cable wire was varied between 8 and 11% that are close to sag ratios of full-scale cables. Additionally, Cases 3b and 4b were tested with a predefined tension and no sag for comparison of wind response between sagged and non-sagged cables.

$$\beta^* = \sin^{-1}(\sin\beta\cos\alpha) \tag{1}$$

where β^* is the equivalent yaw angle of a horizontal cable, and α and β are inclination and yaw angles of an inclined cable on a vertical plane, respectively, β being the angle between the wind direction and the normal axis to the vertical plane of the cable.

2.1. Atmospheric boundary-layer wind profile

In order to properly reproduce the atmospheric boundary layer (ABL) wind profile for a specific terrain, it is required to match the Power law's exponent (α_t), turbulence intensity profile, and wind spectra of the fluctuating wind components u, v, and$w$ with standard values. In the present study, ABL wind profile of an open terrain with α_t= 0.13 was simulated using three spires and three roughness heights distributed from small to large types (see Fig. 4). For validating the simulated terrain, mean wind speed and turbulence intensity profiles are compared in Fig. 4 with those specified in the Architectural Institute of Japan (AIJ) Standard [28] for open terrain, which shows a good agreement. In Fig. 4, mean wind speed (U) and height (Z) are normalized with corresponding values at reference point denoted as U_{ref} and Z_{ref}, respectively, which are associated with 10 m height in the field.

Normalized power spectral densities (PSD) of fluctuating wind components generated in a wind tunnel and those measured in the field need to be similar for keeping the wind characteristics consistent. In this regard, PSD of the fluctuating wind components collected in wind tunnel are compared with empirical spectra suggested by Tieleman [29], which are defined as

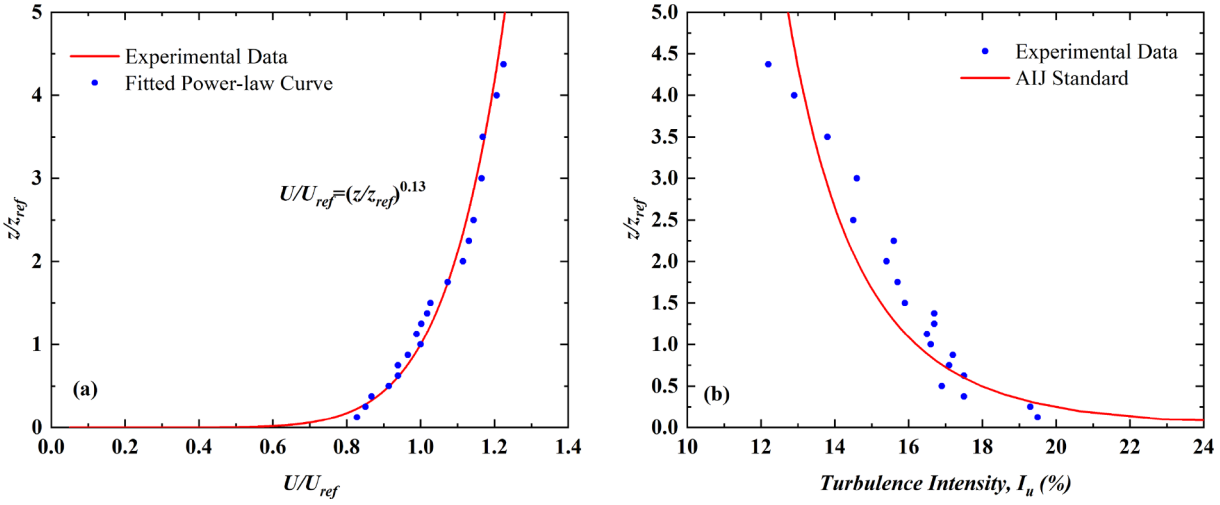

Fig. 4. Comparison of measured ABL wind data with AIJ standard. (a) Mean wind speed profile (b) Turbulence intensity profile.

$$\frac{nS_{uu}(z,\,n)}{\sigma_u^2} = \frac{20.53f}{1 + 475.1f_z^{5/3}} \tag{2}$$

$$\frac{nS_{vv}(z,\,n)}{\sigma_v^2} = \frac{6.83f}{1 + 75.84f_z^{5/3}} \tag{3}$$

$$\frac{nS_{ww}(z,\,n)}{\sigma_w^2} = \frac{6.83f}{1 + 7.23f_z^{5/3}} \tag{4}$$

where S_{uu}, S_{vv}, S_{ww} are the power spectrum of u, v, and w, respectively; n is the frequency in Hertz, and $f_z = nz/U$ is a non-dimensional parameter. Fig. 5 shows the comparison between Tieleman Spectra and PSD of wind components u, v, and w measured at $z = 20$ cm in wind tunnel, which is corresponds to 10 m height in the field based on a length scale of 1:50 used here.

3. Results and discussion

3.1. Experimental data

As described in Section 2, four different cases of a cable with sag were tested to assess the influence of yaw, inclination, and equivalent yaw angles. Apart from these cases, two non-sagged cases were tested to determine the impact of sag ratio on wind-induced response of inclined cables. First and second natural frequencies and mechanical damping ratios for all cases were measured in out-of-plane and in-plane directions through free vibration test, and the results are shown in Table 2. The natural frequency of the cable model corresponding to sagged cases, Cases 1, 2, 3a, and 4a, are slightly different due to slight difference in their initial tensions, and the natural frequencies of non-sagged cases, Cases 3b and 4b, are greater than those of sagged cases because of the increase in cable tension, required to remove the sag.

As mentioned in Section 2, cable's accelerations were measured with two uniaxial accelerometers at each of the two locations along the cable length, Points 1 and 2 (see Fig. 3), and displacements were

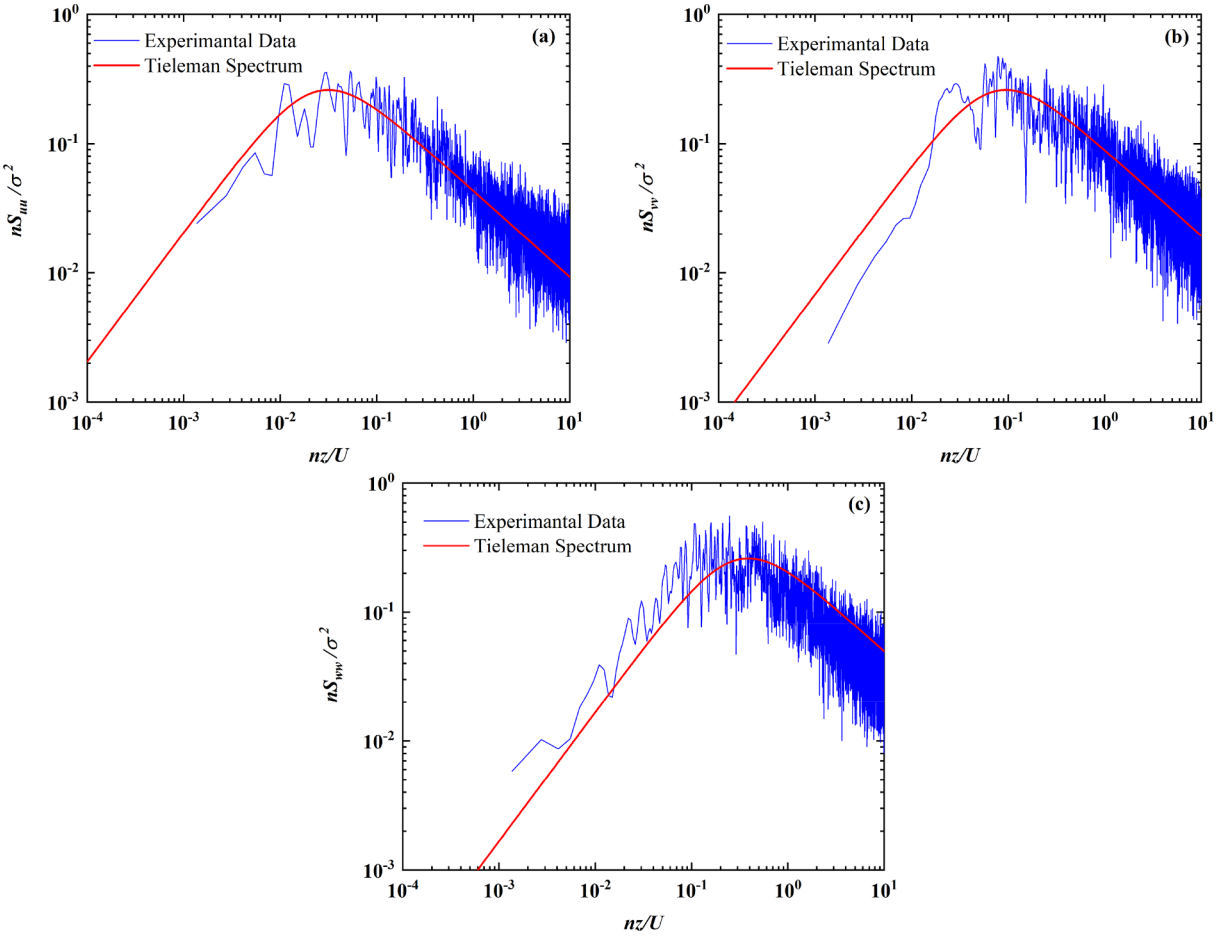

Fig. 5. Comparison of reproduced ABL wind data with Tieleman Spectrum.

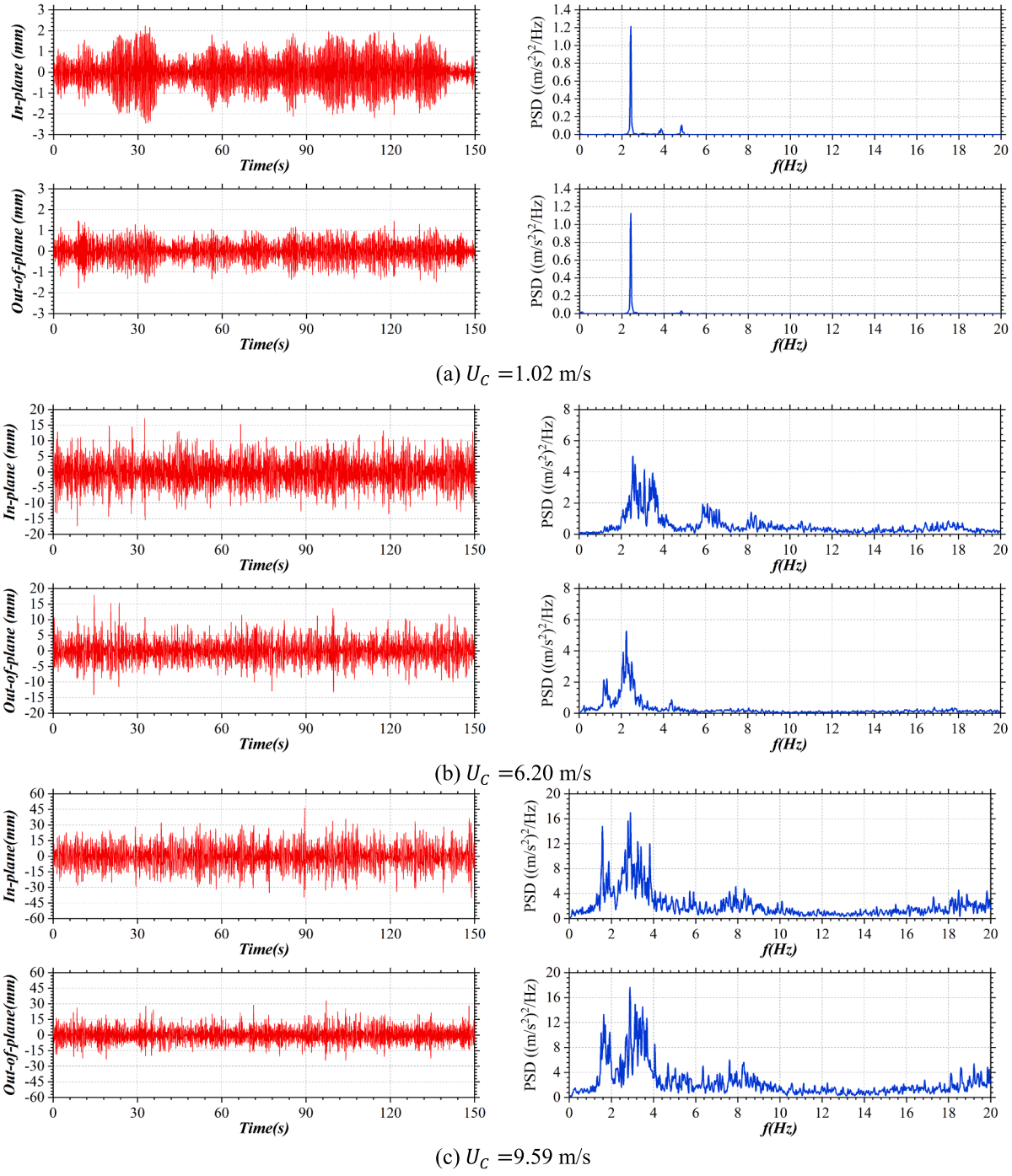

Fig. 6. Time history of displacement and power spectral density of model at three wind speeds -Case 1.

calculated using numerical integration of measured accelerations. Displacements and accelerations reported hereafter are based on data collected at Point 1, but the power spectral density plots are based on acceleration recorded at Point 2. These two locations to report displacement/accelerometer and frequency spectrum were selected based on anticipated excitation modes while keeping the locations consistent between all cases for the sake of comparison. Moreover, Point 1 was chosen as a reference point for data normalization. In Fig. 6, time history of displacement and PSD of acceleration for **Case 1** are shown in both in-plane and out-of-plane directions at low, moderate, and high

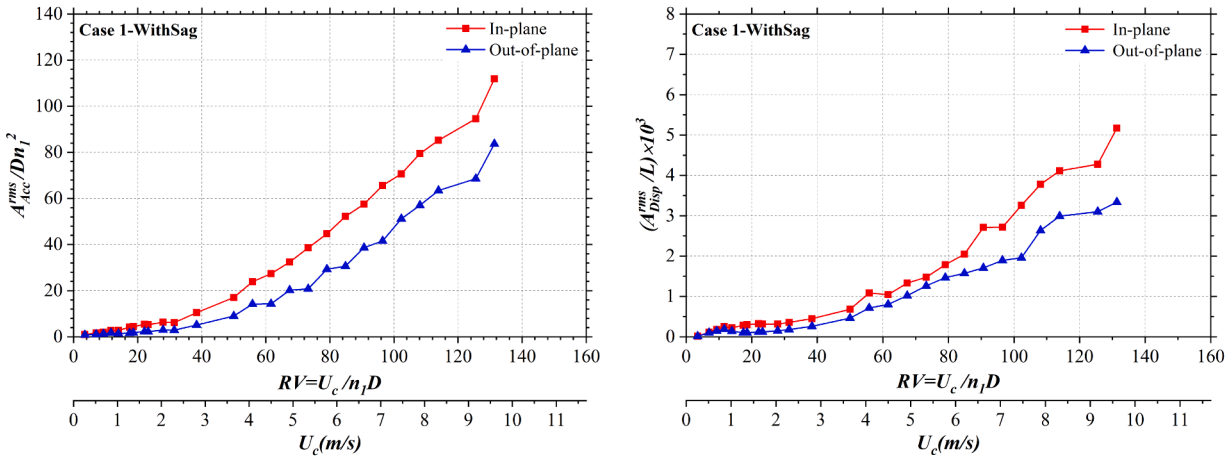

Fig. 7. Normalized root-mean-square of acceleration and displacement-Case 1.

wind speeds tested here. This figure indicates that the cable model in Case 1 mostly vibrates in the second mode at a low wind speed (~1 m/s) while it vibrates in modes 1 and 2 at higher wind speeds (~10 m/s). Furthermore, the PSD results show that the value of dominant natural frequency proportionally increases with wind speed because of increase in cable tension.

The root-mean-square (RMS) of the displacements and accelerations were normalized with cable length (L) and Dn_1^2, respectively, where D is the cable diameter and n_1 is the first natural frequency (in-plane). Fig. 7 shows the cable response in two directions (in-plane and out-of-plane) versus reduced velocity = U_c/n_1D, where U_c is the mean wind speed at Point 1 (mid-point along cable span). It can be seen that in-plane response is greater than out-of-plane response, and the difference eventually becomes significant with increasing reduced velocity. It should be noted that the maximum wind speed for the tests was limited to avoid damage to the model due to excessive vibration.

Fig. 8shows the displacement time history and PSD results for **Case 2**. As shown in Fig. 8, the cable gets excited in the second vibration mode at low wind speed, while the contribution of the first vibration mode appears in addition to the second vibration mode at higher wind speed. This behavior of excitation mode for Case 2 is consistent with Case 1, while they have same inclination angle but different yaw and equivalent yaw angles. Normalized displacement and acceleration of Case 2 are plotted in Fig. 9. Comparison between wind-induced response of Cases 1 and 2 indicates that the displacement amplitude at a given reduced velocity is higher for Case 2 compared with Case 1, which is consistent with a past study [13] and other studies that found the equivalent yaw angle (β^*) of 45° (Case 2) to be more critical than 35° (Case 1).

Structural cables that are used in cable-stayed and suspension bridges or other infrastructures usually have a large sag because of dead weight. In long-span bridges, especially suspension type, sag controls the stability of these long-span structures. Sag ratio, which is denoted as the ratio of maximum static deflection to the span of main cable (S/L), varies from 1/8 to 1/12, with an optimum value of 1/10. Studies indicate that cables with smaller sag ratio make the suspension bridge more stable in vertical direction, but it increases the cable stress due to higher pretension that requires stronger anchorage. Conversely, larger sag ratio for cables reduces the cable tension but requires increasing of the bridge tower's height [30]. As a result, it is essential to investigate the influence of sag ratio on wind-induced vibration of inclined cables. Fig. 10 compares the results of sagged (black color) and non-sagged (red color) cables for **Case 3**. It can be seen from power spectral density plots that the sagged cable (Case 3a) mostly vibrates in the third mode at a low wind speed, while the contribution of first mode shows up at higher wind speeds. While non-sagged cable (Case 3b) shows a dominant peak in the first mode with participation of higher modes at higher wind speeds. Therefore, it can be concluded that cables without sag gets excited not only in the first mode at high wind speeds just like the sagged case, but it differs from its counterpart wherein higher modes also participate, the implication of which would be higher peak stress in the non-sagged cables.

Figs. 11 and 12 are plots of the normalized RMS of accelerations and displacements for **Case 3** with and without sag, respectively. Comparison of obtained results indicates that the wind response of non-sagged cable (Case 3b) in both directions are closer to each other in magnitude than those of a sagged cable (Case 3a). Moreover, the vortex-induced vibration can be observed in Figs. 11 and 12 for wind speed ranging from 1 to 2 m/s. The "lock-in" wind speed range captured here is consistent with those obtained from the Strouhal number equation of an inclined cable presented in a past study ($St = f_s D/U_{vs} = 0.2\cos(\beta^*)$) [13]. It can be seen in Fig. 11b and 12b that while the normalized displacements of sagged and non-sagged cables are similar in value, the normalized accelerations are different at a given wind speed which results in a different first-mode reduced velocity for the two cases due to difference in their fundamental frequency (n_1). The difference in normalized acceleration response by a factor of ~10 cannot be explained based on the difference in the fundamental frequencies of the two cases alone because accelerations are normalized by their respective frequencies. A possible explanation is that the primary mode of

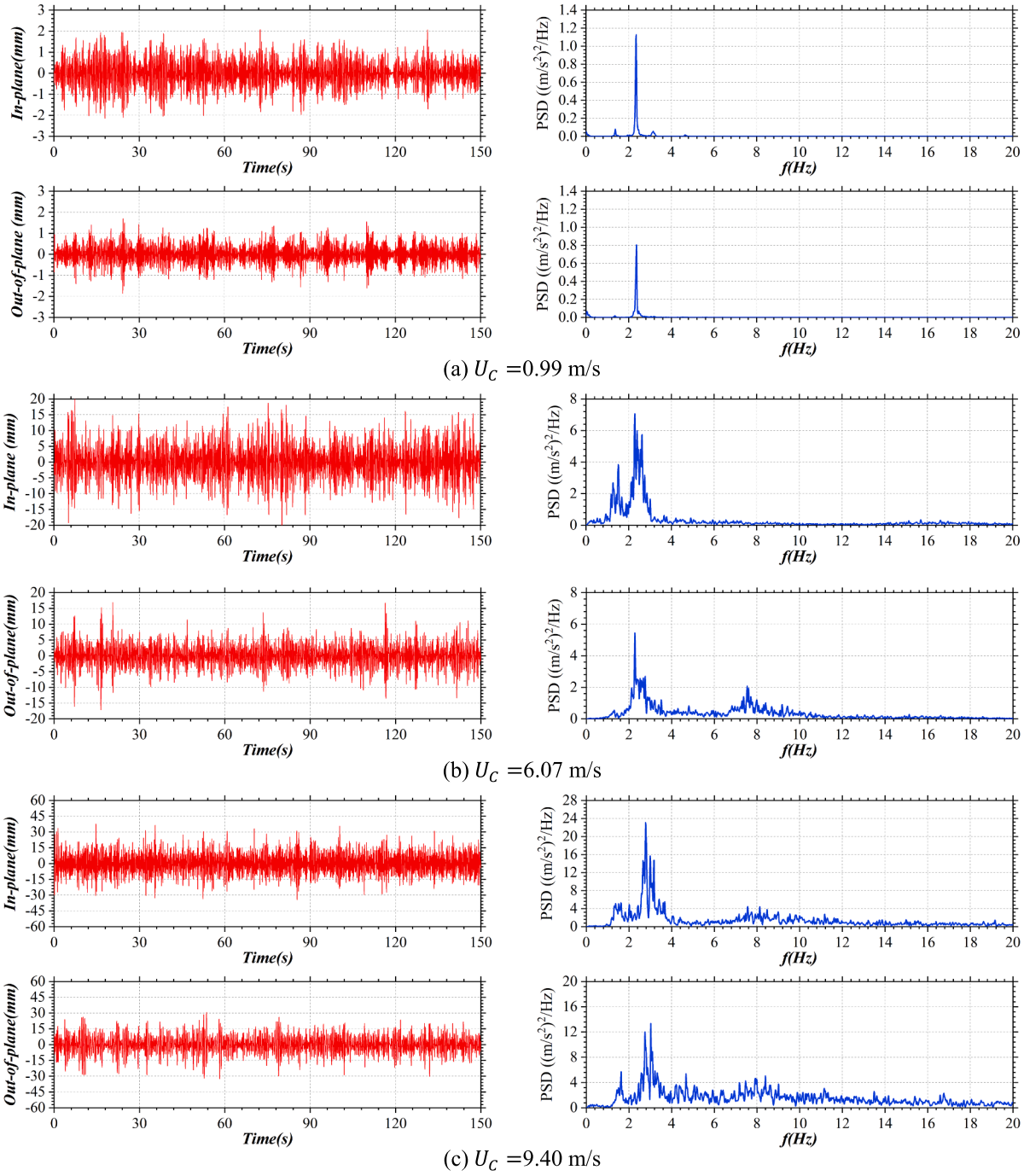

Fig. 8. Time history response of aeroelastic model and power spectral density of acceleration-Case 2.

vibration is first mode in the no-sag case versus second mode in the sag case which should result in four times higher acceleration in the latter with similar displacements between the two cases. The additional factor of 2.5 should be because of difference in the mechanisms of aerodynamic excitation of the cable with the sag versus no-sag.

In another set of experiments, the effects of sag ratio and inclination angle on cable vibration were studied in **Case 4**. In this case, yaw, inclination, and equivalent yaw angles were 35°, 60°, and 45°, respectively. PSD results plotted in Fig. 13 show that the sagged cable (Case 4a) and non-sagged cable (Case 4b) vibrate in the second and first modes, respectively, at a low wind speed while the non-sagged cable also have significant participation of higher modes in addition to the

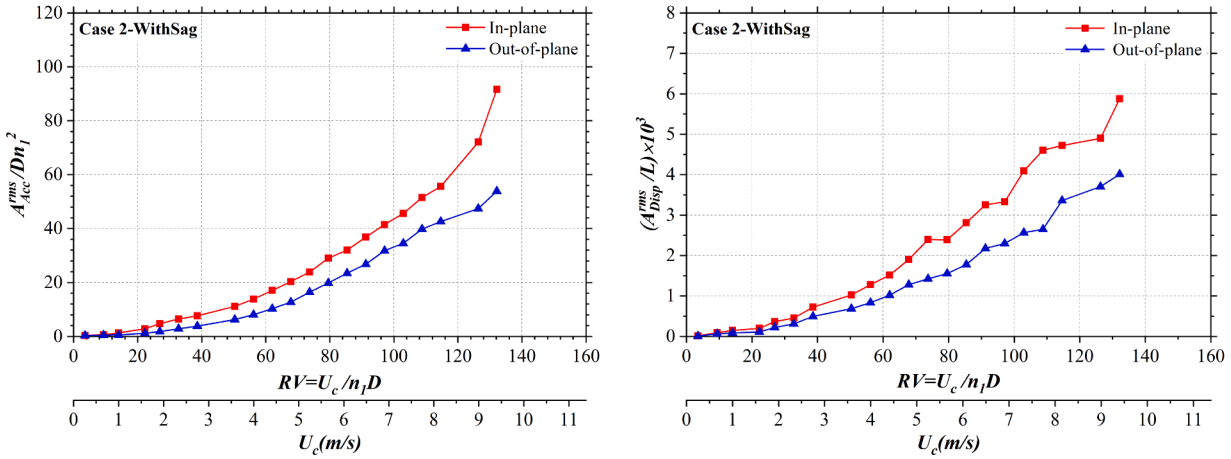

Fig. 9. Normalized root-mean-square of accelerations and displacements at different wind speeds-Case 2.

first mode at high wind speeds. This trend for excitation mode is similar to Case 3, but Cases 1 and 2 followed another trend.

The multi-modal wind-induced response for flexible inclined cables has been observed in past experimental studies [22,31]. In those studies, the contribution of 1st, 2nd, 3rd, and higher modal frequencies was reported for vortex-induced vibration. The participation of higher modes in cable response can be explained through wind speed that varies along the span of an inclined cable because of increasing mean wind speed with elevation in ABL wind. The wind speed gradient along the cable height generates a shear flow that influences the cable's response. The second cause of the observed multi-modal response is buffeting loads on the cable originating from turbulent flow due to the incoming flow and cable excitation that becomes more significant at higher wind speeds. The variation of buffeting loads along the span of the cable because of change in wind turbulence intensity with elevation and span-wise correlation length of wind turbulence along the span of the cable affects its response. The third cause is the cable's natural frequencies that are indirectly related to the sag ratio as increasing the pretension or tensile force in the cable reduces its sag and increases its natural frequencies. This means that a cable with sag is more flexible than the same cable without sag. As it can be seen from the results shown in Figs. 10 and 13, the cable response at low-wind speeds has a single dominant peak for both sag and no-sag cases while the response at higher wind speeds in both the cases has multi-modal components with a broadband type of response, except more so for the cable without sag. Therefore, it can be concluded that the effect of increase in wind speed leads to a multi-modal response in the cables where the cable with sag starts behaving like a cable without sag or a taut cable at higher wind speeds because of increased cable tension or stiffness. Furthermore, it is worth mentioning that the cable with sag is subject to a more complex aerodynamics due to wind-cable interaction that is dependent on the sectional inclination angle of the cable which changes along its length, and perhaps the nonlinearity effects of the interaction show up in its response.

Figs. 14 and 15 indicate the wind response of **Case 4** in the form of normalized accelerations and displacements for both in-plane and out-of-plane directions. Similar to Case 3a, vortex-shedding induced wind excitation of the cable is observed for wind speed ranging from 1 to 2 m/s. The "lock-in" wind speed range captured here is also similar those obtained from the Strouhal number equation of an inclined cable presented in a past study ($St = f_s D/U_{vs} = 0.2\cos(\beta^*)$) [13]. For sagged and non-sagged cables studied in Case 4, similar trend can be observed for wind response that was observed in Case 3a with sag and Case 3b without sag. Furthermore, the results confirms that although increase of cable tension with wind speed increases the natural frequency and thereby changes the reduced velocity, the wind response of both sagged and non-sagged cases are almost similar at a given wind speed. Furthermore, the results confirm that while the normalized displacements of sagged and non-sagged cables are similar, the normalized accelerations are different at a given wind speed in spite of their normalization with the fundamental frequency of the cables that are different. The normalized acceleration response of the sag case is much higher than the no-sag case that can be possibly explained by the difference in their dynamic modes of vibration, which is second mode in sag case and first mode in the no-sag case, and the difference in the mechanisms of aerodynamic excitation of the cable with sag versus no-sag.

A summary of obtained excitation mode(s) based on PSD results for different cases is shown in Table 3.

From this summary table, it can be generally concluded that the inclination angle governs the excitation mode of sagged cables based on the response of the cable in Case 4a versus Case 2 or Case 3a versus Case 1 which are pairs of cables with same equivalent yaw angle but different inclination angle. It is also observed based on the cable response of non-sagged cables (Case 3b and Case 4b) compared to their counterpart sagged cables (Case 3a and Case 4a) that sag plays an important role in determining the dominant excitation mode. The excitation of first mode at all wind speeds and participation of higher modes at higher wind speeds are distinct features observed in non-sagged cables that were not observed in sagged ones.

Natural frequencies of cables depend on the cable tension that is chosen to adjust sag ratio and other design parameters of a cable. Here the cable tensile force was measured in all test cases to track how it changes with wind speed. Fig. 16 presents the cable tensile force (T) of different cases versus reduced velocity corresponding to the first mode. Axial tensile force in the cable is increased for a few cases by as much as ~60%, which results in an increase in the natural frequency of the cable in a particular mode (up to 26.5%). The percentage increase in tension and shift in natural frequencies of a full-scale cable will be

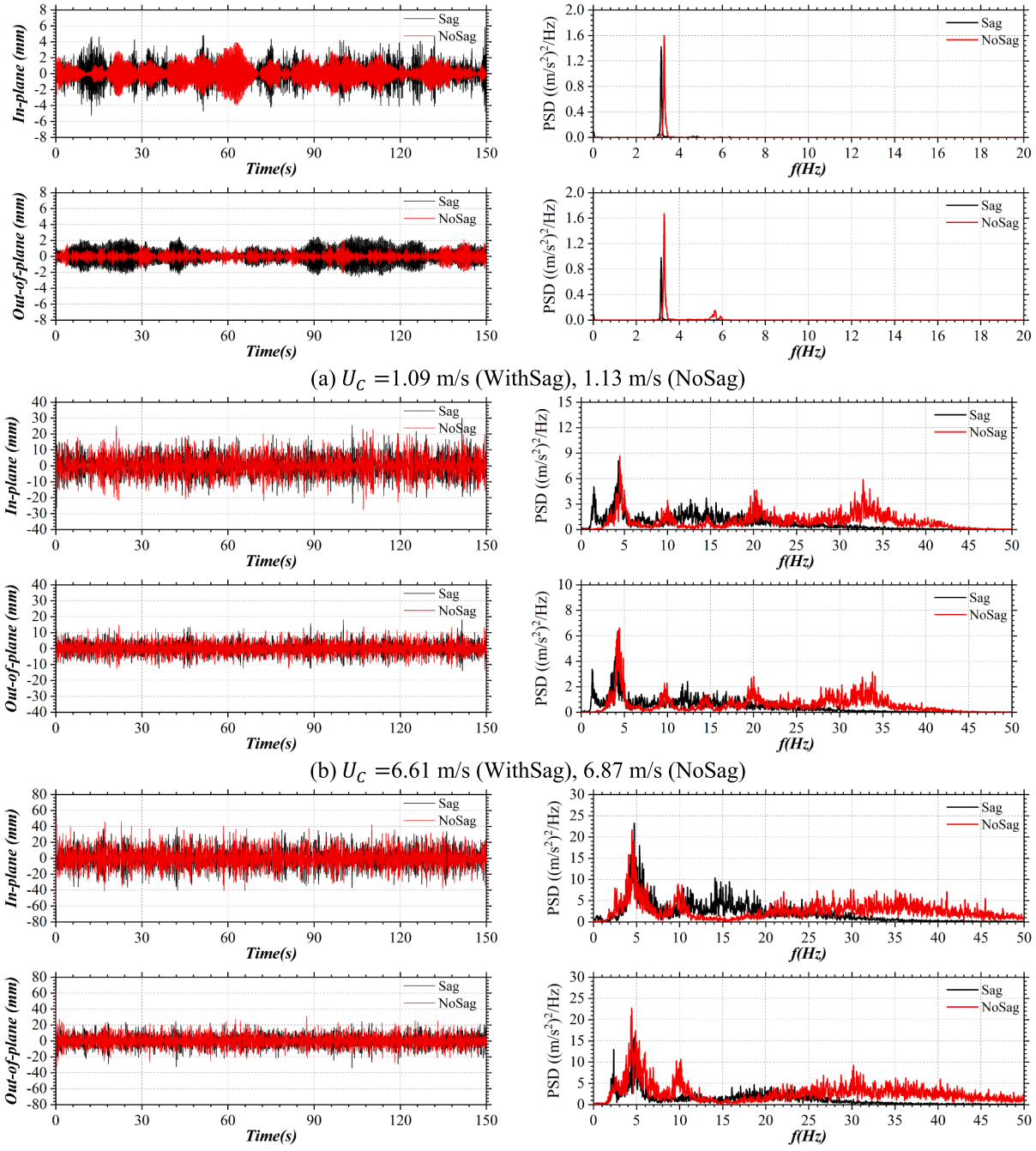

(a) U_C =1.09 m/s (WithSag), 1.13 m/s (NoSag)

(b) U_C =6.61 m/s (WithSag), 6.87 m/s (NoSag)

(c) U_C =10.23 m/s (WithSag), 10.64 m/s (NoSag)

Fig. 10. Comparison of wind response and PSD- Cases 3a- and 3b.

much less than what it was observed here due to having a large initial cable tension in real cables. However, there is some evidence of effect of increased cable tension on the excitation mode either owing to large aerodynamic loads at high wind speeds or increase in pretension given to a cable remove sag as in non-sagged cables. In both cases of sagged cables at high wind speed and non-sagged cables at low wind speed, which have higher cable tension, the first mode was observed to occur. This points out that it could be related to how taut is the cable.

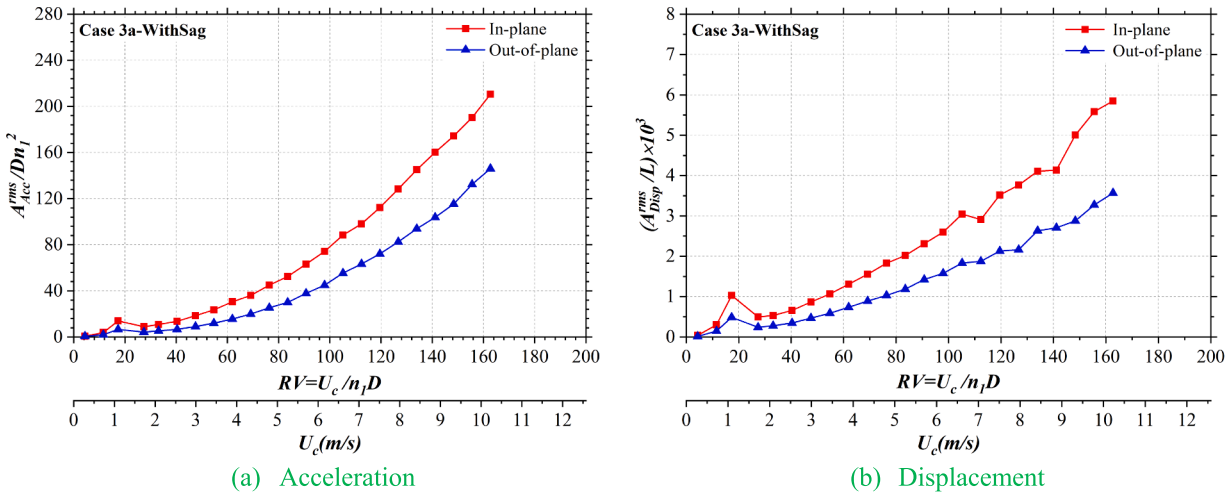

Fig. 11. Normalized root-mean-square of in-plane and out-of-plane accelerations and displacements-Case 3a.

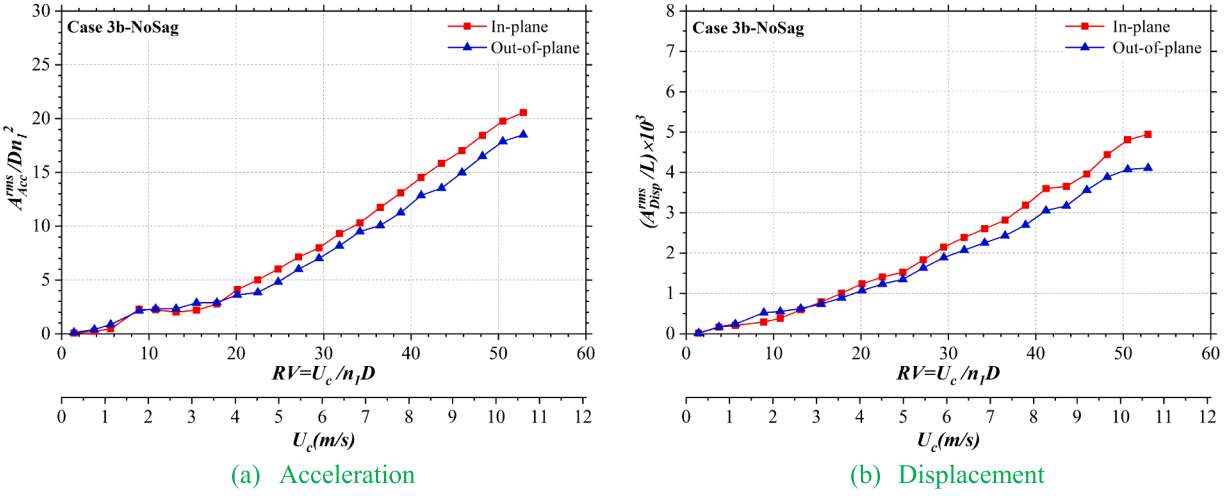

Fig. 12. Normalized root-mean-square of in-plane and out-of-plane accelerations and displacements at different wind speeds-Case 3b.

Studying the motion trajectory of a wind-excited cable is an accepted way to explore the correlation of excited modes as well as phase difference between the two motion directions (in-plane and out-of-plane). Fig. 17 plots the normalized in-plane and out-of-plane accelerations at Point 2 and wind speed $U_C \simeq 10$ m/s. This scatterplot indicates that cable vibration occurs at multiple frequencies, and the elliptical shape of the trajectory reveals the existence of phase change between the two directions, while the inclination of this ellipse proves the equality of dominant excited mode in both directions. This type of motion trajectory for inclined cables has been also reported in past studies on wind-induced cable vibration [22,23].

3.2. Finite element modeling

In this section, the wind load parameters of a yawed cable that were identified by Jafari and Sarkar [13] were used to conduct a study of the vibration response of a full-scale inclined cable through finite element analysis (FEA). The goal here is to check the reliability of using section model results for prediction of critical reduced velocity of an actual cable structure. The experimental results published by Jafari and Sarkar [13] were used to predict the aerodynamic damping and critical reduced velocity of a full-scale cable with sag. Jafari and Sarkar [13] identified the flutter derivatives and buffeting indicial derivative functions of a yawed cable in a wind tunnel for different yaw angles. In this study, ABAQUS software, which is a finite-element-based commercial solver, was used to simulate the self-excited loads. This software was used to take advantage of its features in cable modeling while applying gravitational load and axial force as a predefined load and modeling aeroelastic forces as external aerodynamic damper attached to the cable. Fig. 18 shows all static and dynamic wind loads acting on an inclined sagged cable while there is a yaw angle between wind direction and cable plane. This study focuses only on modeling the self-excited forces acting on a cable to capture the dry-cable galloping instability. In calculating the wind-induced response of a real cable using FEM, one can follow the procedure outlined here where self-excited loads can be included as external dampers attached to the cable and buffeting loads can be included as external loads along with tensile and gravitational loads.

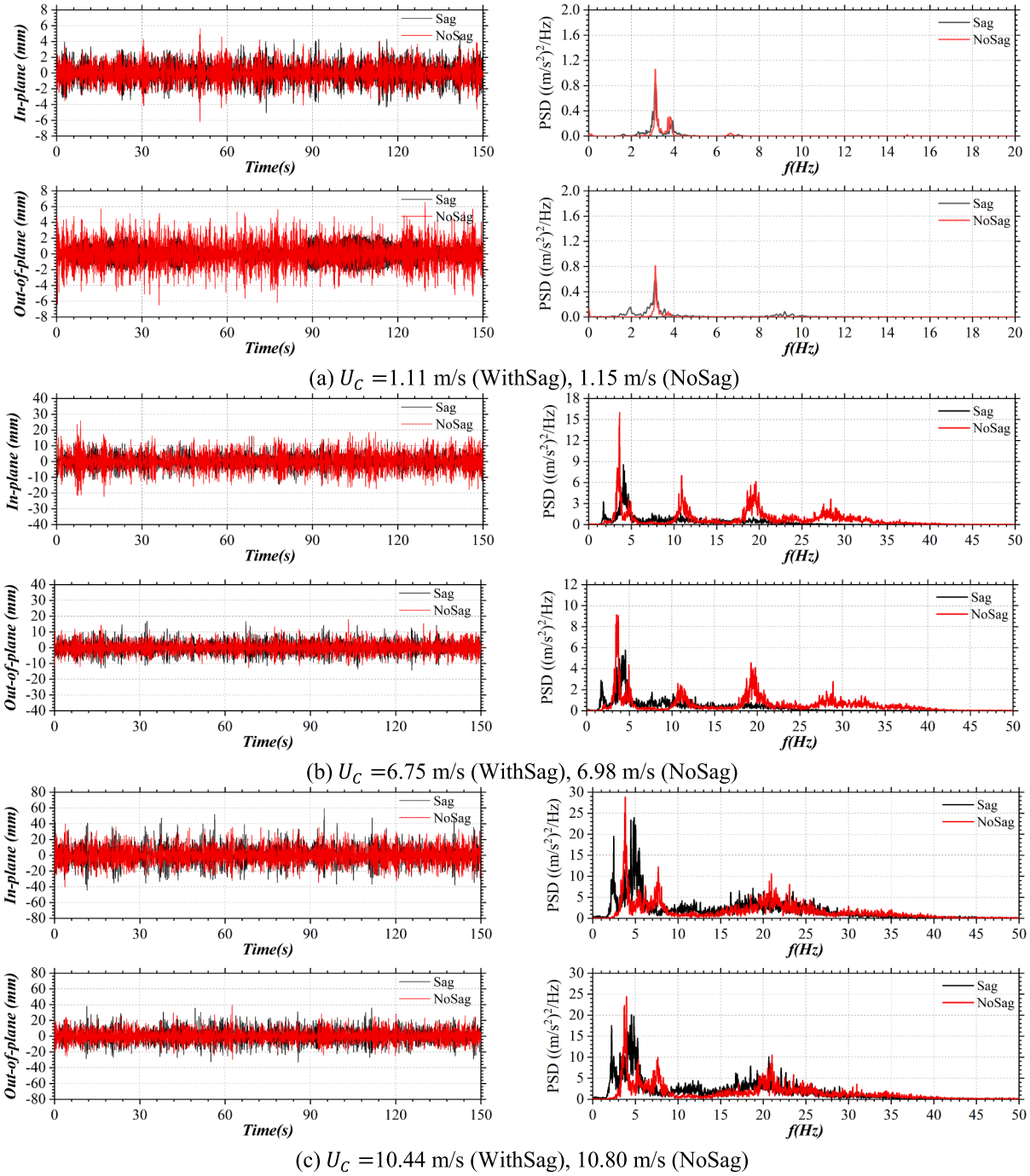

(a) U_C =1.11 m/s (WithSag), 1.15 m/s (NoSag)

(b) U_C =6.75 m/s (WithSag), 6.98 m/s (NoSag)

(c) U_C =10.44 m/s (WithSag), 10.80 m/s (NoSag)

Fig. 13. Comparison of time-history response and PSD results for Case 4 with and without Sag.

3.2.1. Aerodynamic damping identification

The primary aim here is to estimate the wind-induced aerodynamic damping of the full-scale cable while considering the effect of atmospheric boundary layer wind profile, cable geometry, and boundary conditions. For this purpose, a fictitious stay cable of a cable-stayed bridge was selected to identify its aerodynamic damping changes. Table 4 summarizes the details of the selected case for numerical modeling. Before modeling the original case, a validation was

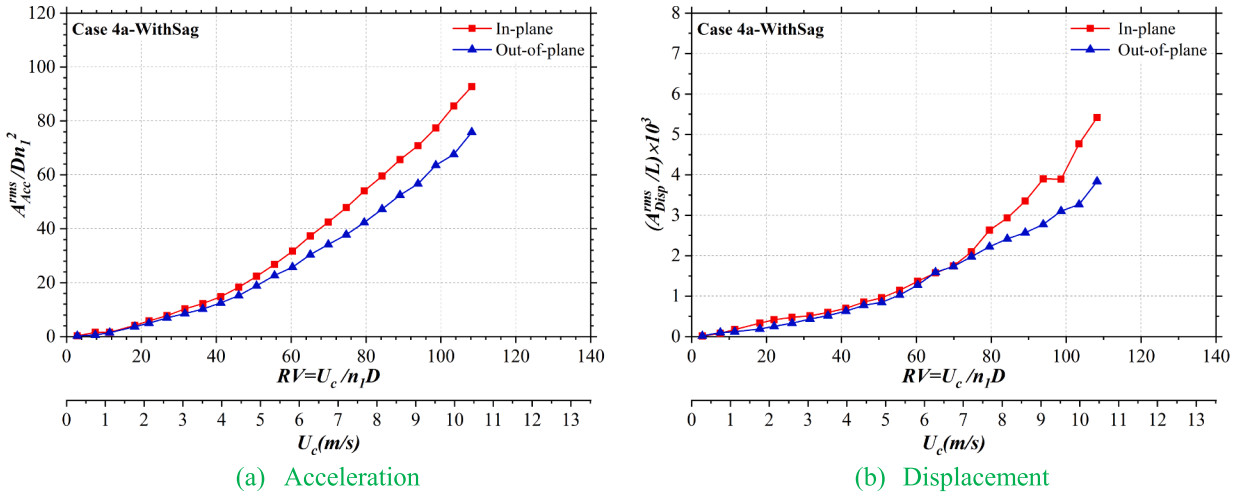

Fig. 14. Normalized in-plane and out-of-plane accelerations and displacements-Case 4a.

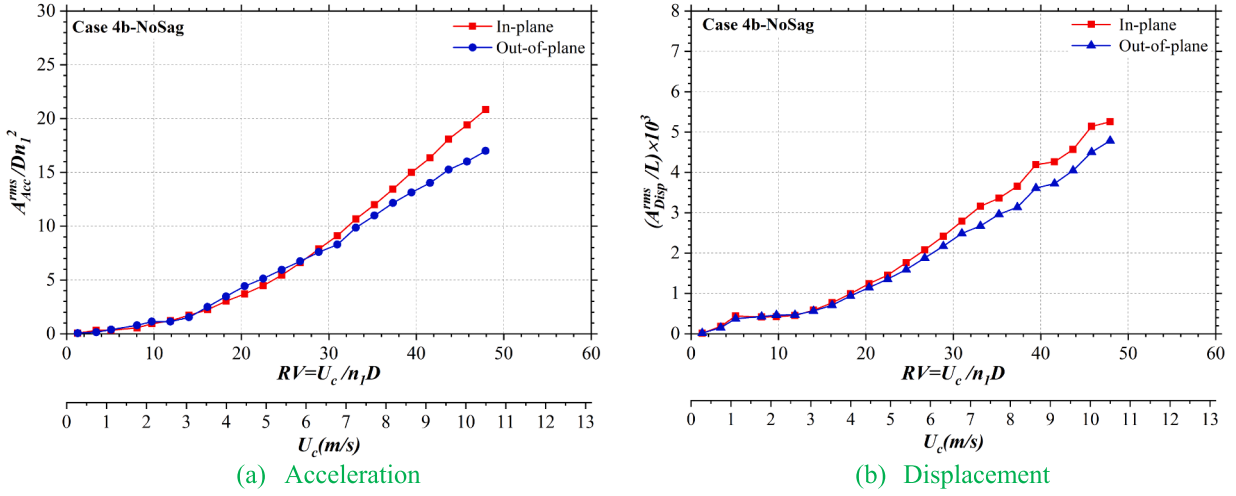

Fig. 15. Normalized in-plane and out-of-plane accelerations and displacements-Case 4b.

Table 3
Summary of observed dominant excited mode(s) in order of contribution for different cases.

Case	Low wind speed	High wind speed
Case 1-WithSag	2nd	2nd & 1st
Case 2-WithSag	2nd	2nd & 1st
Case 3a-WithSag	3rd	3rd & 1st
Case 3b-NoSag	1st	1st & higher
Case 4a-WithSag	3rd	3rd & 1st
Case 4b-NoSag	1st	1st & higher

conducted to evaluate the accuracy of modeling aerodynamic damping especially with negative values as viscous dampers in ABAQUS software. The details of validation are explained in the next section.

3.2.1.1. Validation. For validation of modeling linear viscous damper with a negative damping coefficient to study the onset condition of dry galloping instability that is originated from cable's negative aerodynamic damping in high wind speed, a fixed–fixed beam with a circular cross section including three attached lumped dampers were modeled in ABAQUS (see Fig. 19). The properties of modeled beam and

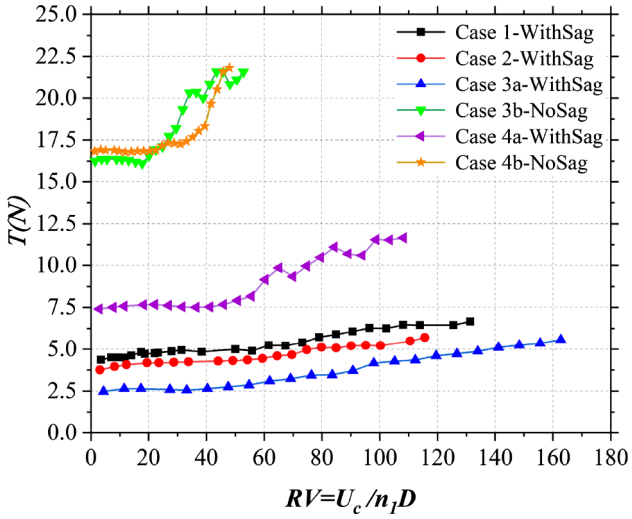

Fig. 16. Effect of wind-induced load on cable's tension for different cases.

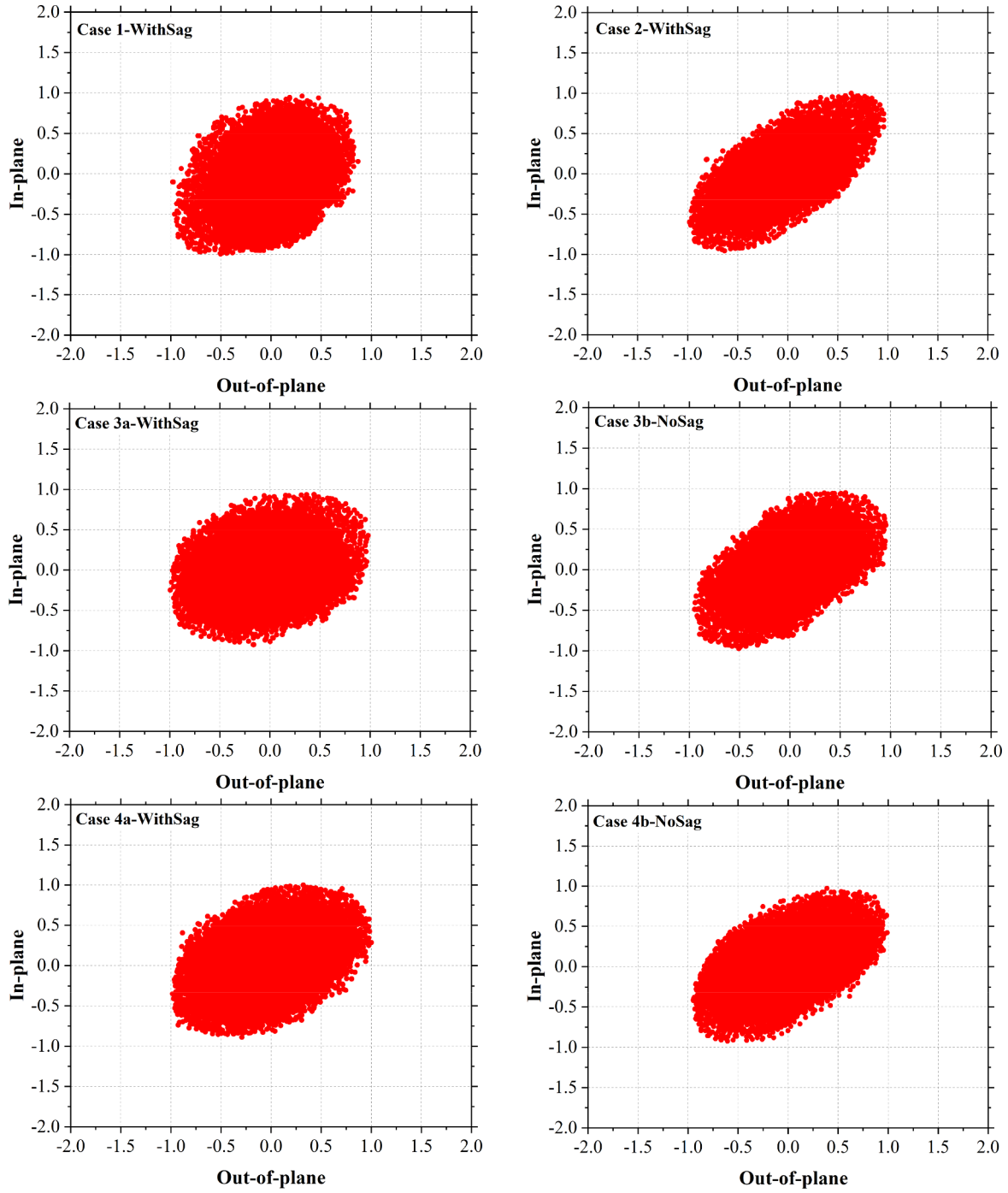

Fig. 17. Normalized motion trajectories of cable for different cases at $U_C \simeq 10$ m/s.

dampers are mentioned in Table 5. After applying an initial displacement of $Y_o = 0.1\ m$ at the mid-point of the beam, its steady-state response was calculated and compared with results taken from numerical analysis using generalized coordinate method for this case (see Fig. 20). This comparison reveals a good match between these two responses that verifies the accuracy of modeling negative-value viscous dampers using connector joint from Interaction Module in ABAQUS. As another validation, the first five natural frequencies of circular beam identified with both these approaches are compared in Table 6, which shows less than 4% error between them.

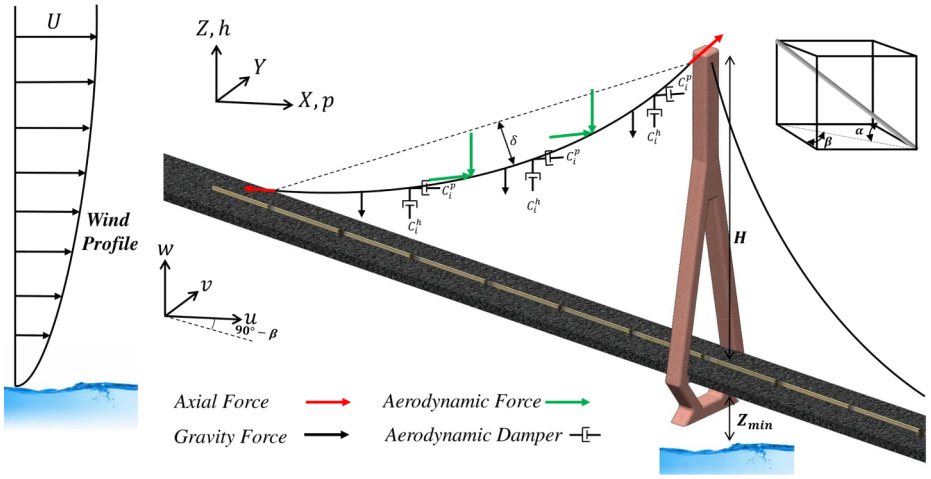

Fig. 18. Schematic view of a cable-stayed bridge exposed to self-excited and buffeting loads.

Table 4
Properties of stay cable of a cable-stayed bridge used for numerical modeling in ABAQUS software.

Parameters	Value
Length, L	100 m
Z_{min}	78 m
Diameter, D	165 mm
Axial load, T	2×10^6 N
Inclination angle, α	35.26°
Yaw angle, β	60°
Equivalent yaw angle, β^*	45°
Elastic modulus, E	200 GPa
Density, ρ	7860 kg/m^3
Mass per unit length, m_e	168.27 kg/m

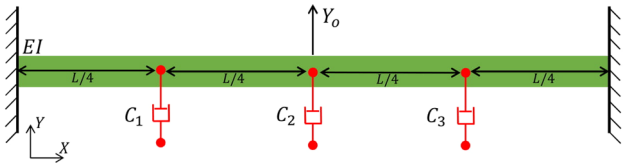

Fig. 19. Schematic view of a fixed–fixed beam with external damper.

Table 5
Properties of simulated circular beam.

Parameter	Value
Young modulus (E)	200 GPa
Length (L)	100 m
Diameter (D)	127 mm
Density (ρ_{st})	7860 kg/m^3
Mechanical damping, ζ	0.05%
Damping coefficient ($C = C_1 = C_2 = C_3$)	−50 N·s/m

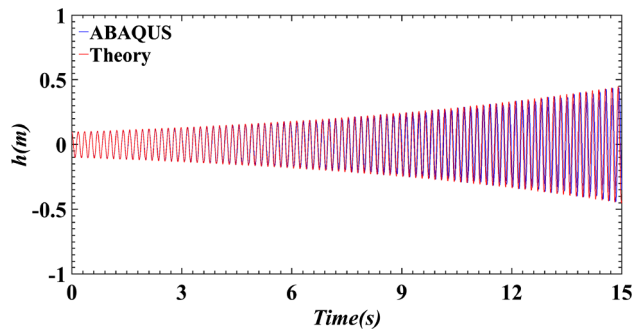

Fig. 20. Comparison of free vibration response using ABAQUS and Theory.

Table 6
Comparison of identified natural frequencies in Hertz from ABAQUS and theory.

Natural Frequency	ABAQUS	Theory
Mode 1	5.699	5.703
Mode 2	15.698	15.720
Mode 3	30.739	30.818
Mode 4	50.739	50.944
Mode 5	75.661	76.102

3.2.1.2. Cable aerodynamic damping. After validation of the procedure to model viscous dampers with negative damping, the original case summarized in Table 4 was used as the cable model with viscous dampers attached at discrete locations in along- and across-wind directions. Pin-pin connection type was used at both ends of the cable while making it free along the axis at one end to apply the axial force. Beam elements were used for the FEA modeling. Fig. 21 shows the grid independency used to determine the appropriate mesh number. It can be seen that the first- and second-mode natural frequencies are unchanged beyond a certain value of mesh size.

Table 7 shows a good consistency between the calculated first five natural frequencies of modeled cable using ABAQUS and Eq. (5) from theory for a non-sagged cable or string.

$$f_q = \frac{q\pi}{L}\sqrt{\frac{EI}{m}\left(\frac{q\pi}{L}\right)^2 + \frac{T}{m}} \tag{5}$$

where f is the natural frequency, q is the vibration mode number, E is the Young module, T is the cable force, L is the cable length, and m is the mass per unit length.

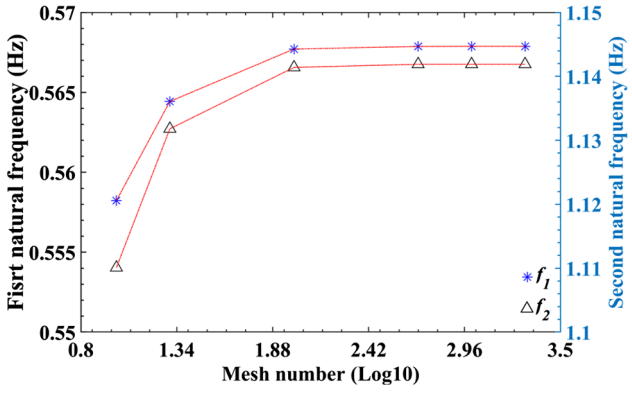

Fig. 21. Grid independency of modeled cable using ABAQUS.

Table 7
Comparison of identified natural frequencies from ABAQUS and theory for modeled full-scale cable.

Natural Frequency, n (Hz)	ABAQUS	Theory
Mode 1	0.568	0.546
Mode 2	1.142	1.098
Mode 3	1.728	1.662
Mode 4	2.332	2.242
Mode 5	2.959	2.846

To calculate the overall aerodynamic damping for this inclined cable, wind profile was generated for a terrain with Power law's exponent of 0.13, and then self-excited load terms were modeled along the cable axis by attaching 16 viscous dampers in along-wind direction and 16 viscous dampers in across-wind direction, which are equally distributed along the cable axis. The damping constants for the dampers in the across-wind and along-wind directions at a given wind speed were found from identified flutter derivatives H_1^* and P_1^* by Jafari and Sarkar [13]. Since stay cables used in the cable-stayed bridges are always in pretension, short cables get excited primarily in the first mode. Hence, the flutter derivatives used in the numerical analysis correspond to the first modal frequency and the wind speed at the location of each damper that depends on the elevation of the node where the damper is attached. The flutter derivatives are converted to the damping terms (C) in across-wind (h) and along-wind (p) directions using $0.5\rho D^2\omega_1 H_1^*(RV$ at desired node) and $0.5\rho D^2\omega_1 P_1^*$ (RV at desired node), respectively. Afterwards, the cable damping, which is purely aerodynamic damping due to defining of zero mechanical damping, was calculated through free vibration test while applying gravitational force and cable axial force, and the wind-induced aerodynamic damping results are shown in Fig. 22. This figure indicates the along- and across-wind aerodynamic damping of an specific inclined cable, as explained in Table 4, for different reduced velocities normalized with wind speed (U_c) located at the mid-point of cable and in-plane natural frequencies (n_1, n_2, n_3). This graph demonstrates that the across-wind aerodynamic damping becomes negative beyond a certain reduced velocity depending on several factors associated with cable properties and wind speed profile.

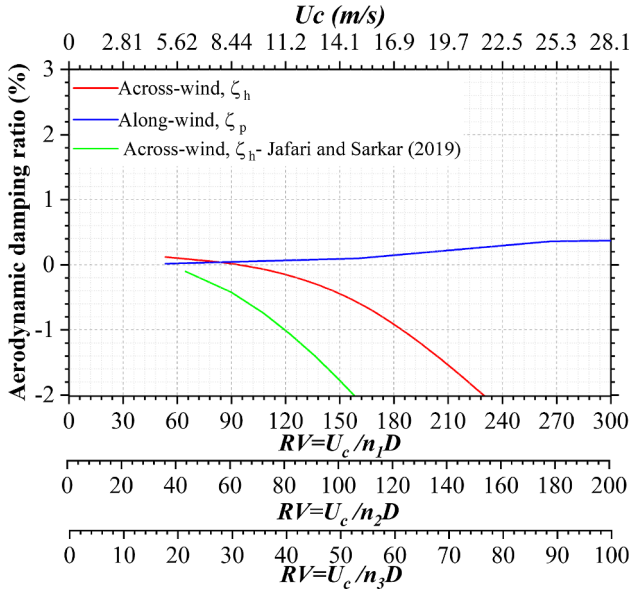

Fig. 22. Aerodynamic damping calculated from numerical simulation.

Instability boundaries for dry cable galloping have been determined in many past studies that are based on section models of cables where the critical reduced velocity for dry galloping is given as a function of Scruton number of the cable. To assess how the predictions of critical reduced velocity (RV_{cr}) based on two-dimensional section model studies would compare with those of a real cable immersed in an atmospheric boundary layer flow, prediction of RV_{cr} from one such past study [13] based on section-model tests for specific yaw angles was compared with the results of the real cable modeled here. The proposed empirical equation for RV_{cr} as a function of Scruton number (Sc), $RV_{cr} = 7.03 * Sc^{0.6} + 46.07$, corresponding to an equivalent yaw angle of $\beta^* = 45^\circ$ for the real cable as in [13] was used to calculate the mechanical damping (ζ_{mech}) of this cable using the $Sc = m\zeta_{mech}/\rho D^2$ of the real cable as needed to prevent dry galloping for a given RV_{cr}. Since total damping that is the summation of mechanical and aerodynamic damping goes to zero at RV_{cr}, the aerodynamic damping (ζ_{aero}) is negative in magnitude of ζ_{mech} for that RV that is plotted in Fig. 22 and compared with the present results for a full-scale cable. These graphs can be used to get the RV_{cr} for a given mechanical damping (ζ_{mech}) that is taken equal to negative of the aerodynamic damping (ζ_{aero}). For a specific aerodynamic damping (magnitude), it can be seen that the critical reduced velocity RV_{cr} of the full-scale cable is higher than the one predicted by section model tests. For example, if $\zeta_{mech} = 1\%$ then $\zeta_{aero} = -1\%$ will give $RV_{cr} = 120$ (1st mode) based on section model and$RV_{cr} = 186$ (1st mode) based on numerical simulation of full-scale cable damping (across-wind). This means consideration of other factors such as wind speed profile, boundary conditions, etc., is needed to accurately predict the critical reduced velocity for galloping of an inclined cable. Furthermore, it is required to know the excitation mode for defining the critical reduced velocity as seen in this plot.

4. Conclusions

Inclined smooth cables that are used to secure the main structure have different applications including but not limited to cable-stayed and tied-arch bridges, and suspended roofs. Structural cables exposed to extreme wind-induced loads experience moderate to large-amplitude vibrations because of their low inherent damping. The vulnerability to wind-induced vibration can cause catastrophic damage or even failure of the structure secured by cables. In this regard, it is crucial to explore the aeroelastic behavior of the long-span cables in atmospheric boundary layer wind. In this study, a series of wind tunnel tests were performed on a newly designed aeroelastic model of a flexible cable to better understand the wind-induced response of a full-scale cable in extreme wind such as hurricane and thunderstorm. For this purpose, the effects of different parameters including sag ratio and wind directions were studied in an atmospheric boundary layer wind with mean wind speed and turbulence intensity profiles of an open terrain. Wind response was measured for a range of wind speeds using four accelerometers attached to the model. Cable tensile force was also monitored during all experiments to find the correlation of wind speed, excited mode, and natural frequency of the cable due to the change in cable tension. In the second part of this study, a series of finite element analyses were conducted to estimate the wind-induced aerodynamic damping of an inclined full-scale cable. The results from the aeroelastic model study indicated that excitation mode primarily depends on inclination angle, sag ratio, and wind speed. For all cases, first, second, third vibration modes appeared at low wind speed, and higher modes were observed at high wind speed. The results indicate that cable tensile force dramatically increases with wind speed and results in increase in the value of cable's natural frequency due to increase in stiffness. It was also found from numerical analysis that the section-model-based

criterion is more conservative to predict the critical reduced velocity for dry galloping instability, i.e. predicts a smaller critical value. Neglecting the effect of parameters such as wind speed profile, boundary conditions, axial and gravity forces, and mode shape contribution can be the reason why section-model-based criterion is more conservative.

Acknowledgement

The authors gratefully acknowledge the U.S. National Science Foundation (NSF) for financially supporting this research under grant # CMMI-1537917.

References

[1] Martins FAC, Avila JPJ. Effects of the Reynolds number and structural damping on vortex-induced vibrations of elastically-mounted rigid cylinder. Int J Mech Sci 2019;156:235–49.
[2] Xu W, Ma Y, Cheng A, Yuan H. Experimental investigation on multi-mode flow-induced vibrations of two long flexible cylinders in a tandem arrangement. Int J Mech Sci 2018;135:261–78.
[3] Liu M, Yang W, Chen W, Xiao H, Li H. Experimental investigation on vortex-induced vibration mitigation of stay cables in long-span bridges equipped with damped crossties. J Aerosp Eng 2019;32:1–10.
[4] Li H, Chen WL, Xu F, Li FC, Ou JP. A numerical and experimental hybrid approach for the investigation of aerodynamic forces on stay cables suffering from rain-wind induced vibration. J Fluids Struct 2010;26:1195–215.
[5] Wang J, Lu P, Bi JH, Guan J, Qiao HY. Three-phase coupled modelling research on rain-wind induced vibration of stay cable based on lubrication theory. J Fluids Struct 2016;63:16–39.
[6] Ge Y, Chang Y, Xu L, Zhao L. Experimental investigation on spatial attitudes, dynamic characteristics and environmental conditions of rain–wind-induced vibration of stay cables with high-precision raining simulator. J Fluids Struct 2018;76:60–83.
[7] Jing H, Xia Y, Li H, Xu Y, Li Y. Excitation mechanism of rain–wind induced cable vibration in a wind tunnel. J Fluids Struct 2017;68:32–47.
[8] He X, Cai C, Wang Z, Jing H, Qin C. Experimental verification of the effectiveness of elastic cross-ties in suppressing wake-induced vibrations of staggered stay cables. Eng Struct 2018;167:151–65.
[9] Zhang D, He Z, Huang Z, Jiang W. Isogeometric collocation method for the galloping of an iced conductor. J Eng Mech 2017;143:04017009.
[10] Demartino C, Ricciardelli F. Assessment of the structural damping required to prevent galloping of dry HDPE stay cables using the quasi-steady approach. J Bridg Eng 2018;23:1–17.
[11] Tokoro S, Komatsu H, Nakasu M, Mizuguchi K, Kasuga A. Study on wake-galloping employing full aeroelastic twin cable model. J Wind Eng Ind Aerodyn 2000;88:247–61.
[12] Matsumoto M, Yagi T, Hatsuda H, Shima T, Tanaka M, Naito H. Dry galloping characteristics and its mechanism of inclined/yawed cables. J Wind Eng Ind Aerodyn 2010;98:317–27.
[13] Jafari Mohammad, Sarkar Partha P. Parameter identification of wind-induced buffeting loads and onset criteria for dry-cable galloping of yawed/inclined cables. Eng Struct 2019;180:685–99.
[14] Cheng S, Irwin PA, Tanaka H. Experimental study on the wind-induced vibration of a dry inclined cable-Part II: Proposed mechanisms. J Wind Eng Ind Aerodyn 2008;96:2254–72.
[15] Cheng S, Larose GL, Savage MG, Tanaka H, Irwin PA. Experimental study on the wind-induced vibration of a dry inclined cable-Part I: Phenomena. J Wind Eng Ind Aerodyn 2008;96:2231–53.
[16] Benidir A, Flamand O, Dimitriadis G. The impact of circularity defects on bridge stay cable dry galloping stability. J Wind Eng Ind Aerodyn 2018;181:14–26.
[17] Duy HV, Katsuchi H, Yamada HNM. Experimental study on dry-state galloping with various wind relative angles and its countermeasures. J Struct Eng 2014;60A:428–36.
[18] Yeo DJN. A mechanism for large amplitude, wind-induced vibrations of stay cables. Proc. 11th Am. Conf. Wind Eng. San Juan. 2009.
[19] Wu X, Sharma A, Jafari MSP. Towards predicting dry cable galloping using detached eddy simulations. 55th AIAA Aerosp. Sci. Meet. 2017. p. 1483.
[20] Wu X, Jafari M, Sarkar P, Sharma A. Verification of DES for flow over rigidly and elastically-mounted circular cylinders in normal and yawed flow. J Fluids Struct 2020;94:102895.
[21] Raeesi A, Cheng S, Ting DSK. Application of a three-dimensional aeroelastic model to study the wind-induced response of bridge stay cables in unsteady wind conditions. J Sound Vib 2016;375:217–36.
[22] Chen WL, Zhang QQ, Li H, Hu H. An experimental investigation on vortex induced vibration of a flexible inclined cable under a shear flow. J Fluids Struct 2015;54:297–311.
[23] Gao D, Chen WL, Zhang RT, Huang YW, Li H. Multi-modal vortex- and rain–wind-induced vibrations of an inclined flexible cable. Mech Syst Signal Process 2019;118:245–58.
[24] Belloli M, Collina A, Rosa L, Squicciarini G. Wind tunnel tests on different erection stages of a cable stayed bridge. Proc 8th Int Conf Struct Dyn EURODYN. 2011. p. 1325–32.
[25] Khrapunov E, Solovev S. Ensuring the aerodynamic stability of the long-span bridges through studies in the wind tunnel. MATEC Web Conf. 2018. p. 245.
[26] Cluni F, Gusella V, Ubertini F. A parametric investigation of wind-induced cable fatigue. Eng Struct 2007;29:3094–105.
[27] Matsumoto M. Effects of axialflow and Karman vortex interference on dry-state-galloping of inclined stay-cables. Proc. 6th Int. Symposium cable Dyn.. 2005.
[28] Architectural Institute of Japan (AIJ). AIJ recommendations for loads on buildings. Architectural Institute of Japan; 1996.
[29] Tieleman HW. Universality of velocity spectra. J Wind Eng Ind Aerodyn 1995;56:55–69.
[30] Lin W, Yoda T. Bridge engineering: classifications, design loading, and analysis methods. Butterworth-Heinemann; 2017.
[31] Huera-Huarte FJ. Multi-mode vortex-induced vibrations of a flexible circular cylinder. Imperical College London; 2006.